Nationaal Lucht- en Ruimtevaartlaboratorium
National Aerospace Laboratory NLR

NLR TP 96284

Flow field survey in trailing vortex system behind a civil aircraft model at high lift

A.C. de Bruin, G.H. Hegen, P.B. Rohne and Ph.R. Spalart

DOCUMENT CONTROL SHEET

	ORIGINATOR'S REF.		SECURITY CLASS.
	TP 96284 U		**Unclassified**

ORIGINATOR
National Aerospace Laboratory NLR, Amsterdam, The Netherlands

TITLE
Flow field survey in trailing vortex system behind a civil aircraft model at high lift

PRESENTED AT
78th AGARD Fluid Dynamics Panel Meeting and Symposium on "The Characterisation and Modification of Wakes from Lifting Vehicles in Fluids", 20-23 May 1996, in Trondheim

AUTHORS	DATE	pp	ref
A.C. de Bruin, G.H. Hegen, P.B. Rohne, Ph.R. Spalart	**960424**	**14**	**A**

DESCRIPTORS

Aircraft wakes	**Vortices**
Flow visualization	**Vorticity equations**
Flow measurement	**Wind tunnel tests**
Lift devices	**Wind tunnel models**
Transport aircraft	**Wing tips vortices**

ABSTRACT
The roll-up of the trailing vortex system behind a generic civil aircraft windtunnel model with extended flaps and slats is studied up to 5 wing spans downstream. A laser light sheet flow visualisation technique is used and detailed flow field measurements are made with a spanwise traversable rake with five-hole probes. The measurement results are compared against calculations with the 2D vorticity transport equation.

Contents

Flow field survey in trailing vortex system behind a civil aircraft model at high lift

Anton C. de Bruin, Sinus H. Hegen, P. Bernd Rohne
National Aerospace Laboratory NLR
Voorsterweg 31, 8316 PR Marknesse, the Netherlands
and
Philippe R. Spalart
Boeing Commercial Airplane Group
P.O. Box 3707, M/S 67-LM, Seattle WA 98124-2207, USA.

SUMMARY
The roll-up of the trailing vortex system behind a generic civil aircraft windtunnel model with extended flaps and slats is studied up to 5 wing spans downstream. A laser light sheet flow visualisation technique is used and detailed flow field measurements are made with a spanwise traversable rake with five-hole probes. The measurement results are compared against calculations with the 2D vorticity transport equation.

LIST OF SYMBOLS

b	wing span of the model (b=1.3565 m)
u,v,w	non-dimensional velocity components
$c_l c$	local wing load
r	non-dimensional distance to vortex core
C_L	lift coefficient
MRP	Model Reference Point
Re_b	Reynoldsnumber
S	wing area
X_{MRP}	position of MRP at α=0 deg
Xb	downstream position in wake $(X-X_{MRP})/b$
Yb,y	spanwise position (Y/b)
Zb,z	vertical position (Z/b)
α	angle of attack of model (deg)
ω_x	non-dimensional streamwise vorticity
Γ	non-dimensional bound circulation
Ψ	streamfunction for crossflow velocity components

1. INTRODUCTION
The trailing vortex system behind civil aircraft may have important implications for trailing aircraft. In particular during the take-off and landing phase where, due to increased airport congestion, separation distance between individual aircraft tends to be small. In the present study the development of the wake roll-up behind a high-lift model with part-span flaps and slats is followed up to 5 wing spans downstream. Flow visualisations with the laser light sheet method reveal a stable vortex system with vortices emanating from the wing tip, the edge of the outboard flap and the edge of the inboard flap. In addition detailed flow field measurements with a rake with five-hole probes enable a more quantitative analysis of the wake roll-up process. Measured data-fields are analysed for the downstream development of axial velocity, streamwise vorticity and circulation. Measured streamwise vorticity fields are used to check the validity of the two-dimensional vorticity transport equation. Additional experiments are planned in the large low speed windtunnel DNW, to obtain data up to about 13 wing spans downstream of the model.

2. EXPERIMENTAL SET-UP

2.1 Windtunnel
The Phase I and Phase II experiments were performed in NLR's closed circuit low speed windtunnel LST which has a cross section of 3.0x2.25 m^2 and a test section length of 8.75 m with excellent visual accessibility through removable transparent side panels. The LST windtunnel has a remarkably low free stream turbulence level of about .025%. It is equipped with a remote controlled Y-Z traversing mechanism, allowing manual movements in X-direction over most of the test section length. Additional Phase III experiments are planned in the large (8x6 m^2) low speed tunnel DNW. All tests are made at 60 m/s.

2.2 Model
An existing generic civil aircraft model was used, it consists of a fuselage and a wing only (fins and engines were not mounted). Figure 1 gives a sketch of wing planform and the flap and slat system. The measurements concentrate on a model geometry with a strong 35 degrees deflected inboard flap. The aft part of the flap has an extra flap partition, the inboard part has an extra deflection of 10 deg. The outboard flap was deflected either 5 or 15 degrees. Table 1 gives a summary of the investigated model configurations. To give an impression of measured lift coefficients for the various model configurations investigated, C_L-α polars are shown in figure 2. The maximum lift coefficient is about 2 with flaps extended, while with flaps and slats a value of about 3 is reached. Flow field measurements concentrate on model configurations 2 and 5.

Table 1 Model configurations

Conf.	Test Phase		deflection (deg)	
			slat	flap
	I	II	inner/outer	inner/outer
7	X	-	0 / 0	0 / 0
2	X	X	0 / 0	35-10/0 / 5
3	X	-	0 / 0	35-10/0 / 15
5	X	X	10 / 20	35-10/0 / 5
6	X	-	10 / 20	35-10/0 / 15

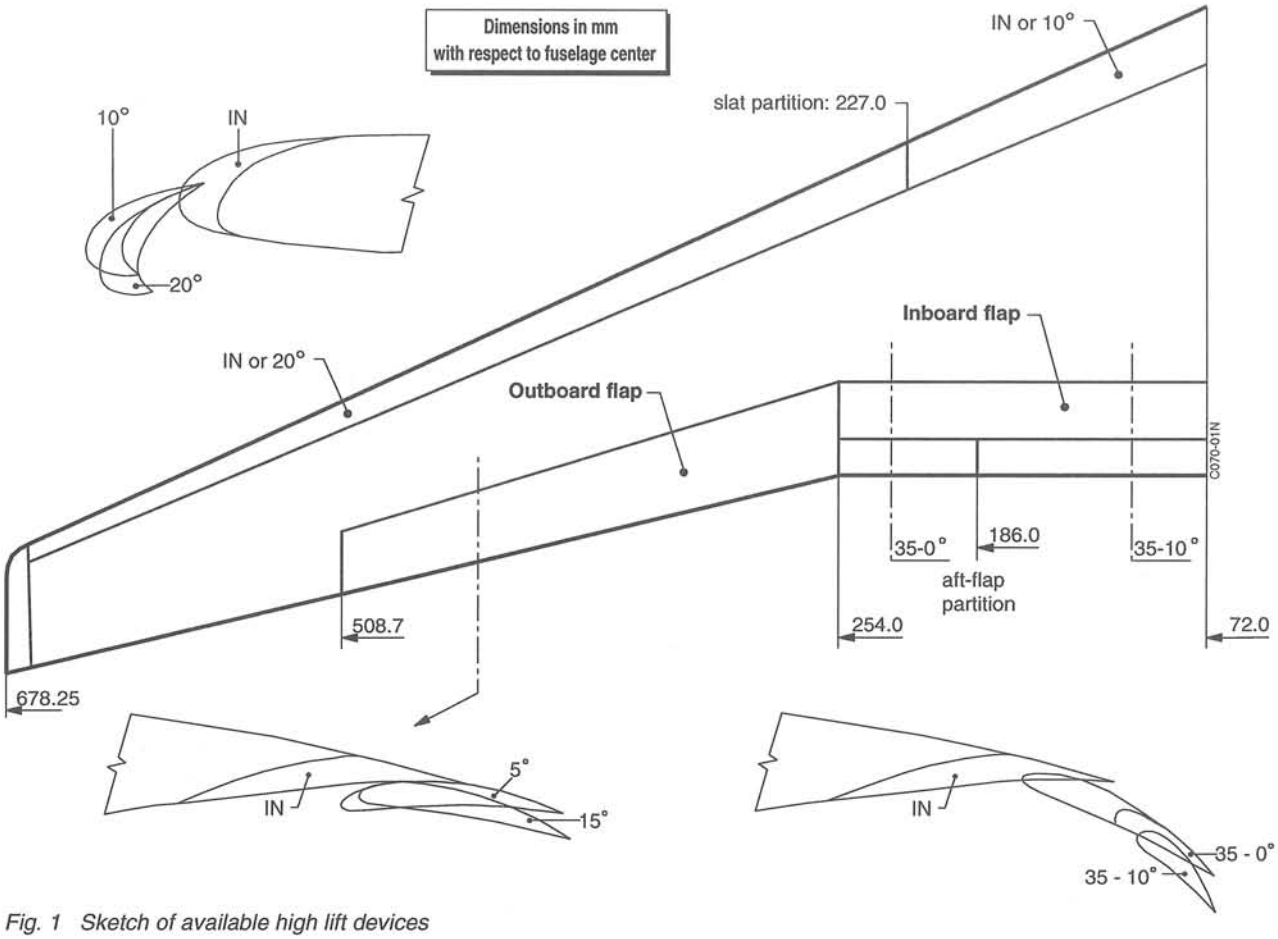

Fig. 1 Sketch of available high lift devices

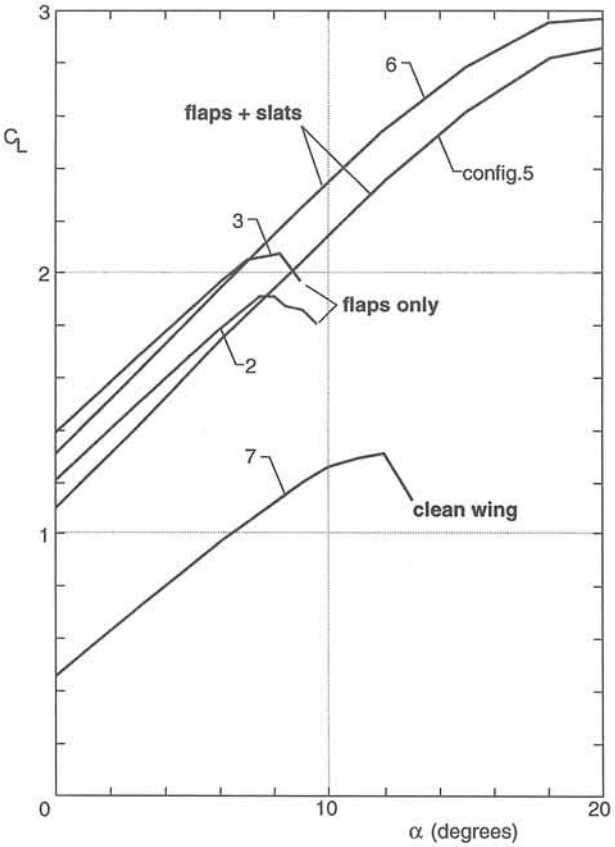

Fig. 2 C_L - α curves

The model is mounted on a subsonic sting support connected to the wind tunnel floor via a manually controlled alpha mechanism interface. Model forces are measured with an internal balance. The model is positioned close to the test section entrance to obtain maximum distance downstream of the model. Only symmetric flow conditions are considered. Non-dimensional downstream position in the wake is referenced to the nominal (α=0 deg) position of the Model Reference Point: $Xb=(X-X_{MRP})/b$. At α=0 deg the fuselage centerline is at Zb=0.153 above the windtunnel centerline.

2.3 Laser screen flow visualisation

In the Phase I tunnel entry, a laser light sheet flow visualisation method was used. Smoke is injected at an appropriate location just upstream of the model. By moving the smoke tube progressively in-board, the individual vortices emanating from the wing tip and the flap edges are identified, even at

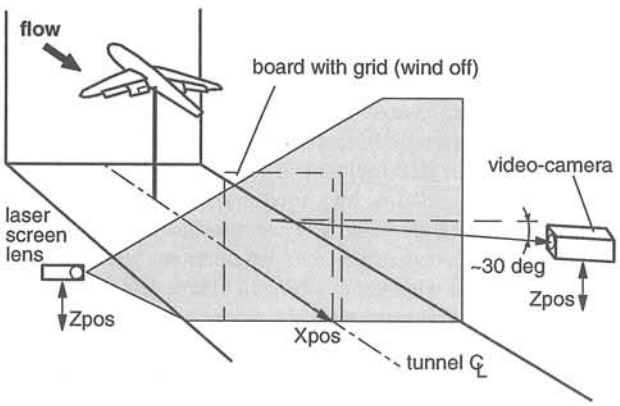

Fig. 3 Set-up for laser screen visualization in LST

Table 2 Visualisation tests (Phase I)

Conf.	Xb	α (deg)
2	.68, 1.2, 2.0, 3.3, 5.0	7
5	.68, .86, 1.2, 2.0, 3.3, 5.0	18
6	.86, 1.2, 2.0, 3.3, 5.0	18
3	.68, .86, 1.2, 2.0, 3.3, 5.0	7
3	5.0	4, 5, 6
7	.68, .86, 1.2, 2.0, 3.3, 5.0	10

long distances downstream of the model. The video camera and the screen emitting lens are mounted on the traversing mechanism, but at opposite sides of the tunnel test-section (see Fig. 3). Individual vortex cores appear as black holes in the video images. At the Xb locations given in table 2 the Yb and Zb position (with respect to the tunnel axis) of the individual vortex cores is evaluated from video-still images.

2.4 Flow field measurements

Preliminary flow field measurements were made during Phase I, while more extensive flow field measurements were made in the Phase II tunnel entry (see Tab. 3). A NLR designed and built rake equipped with 18 miniature five-hole probes with spherical heads is used (Ø2.5 mm, probe pitch of 15 mm, see Fig. 4). Probe pressures are electronically scanned (with the electronically scanned pressure units placed inside the rake support sting) yielding high data rates with on-line pressure calibration abilities. The rake sting is mounted on a streamlined horizontal strut, which penetrates the windtunnel side walls, and is fixed to the Y-Z traversing mechanism (see Fig. 5). The rake is continuously traversed in spanwise Y-direction (traversing speed 5 mm/s), while taking measurements every

Table 3 Flow field measurements (Phase II)

Conf.	α (deg)	Xb			
		.67	2.00	3.53	4.69
2	3	.34/.53	-	-	.37/.33
2	5	.34/.53	-	-	.34/.34
2	7	.34/.55	.35/.50	.33/.46	.35/.39
2	9	.33/.59	-	-	.35/.39
5	9	.33/.55	-	-	.33/.38
5	12	.33/.55	-	-	.31/.42
5	15	.33/.59	-	-	.29/.44
5	18	.32/.60	.28/.52	.27/.47	.26/.45

Note: tabulated data refer to non-dimensional distance of tip and inboard flap vortex and maximum cross-flow velocity.

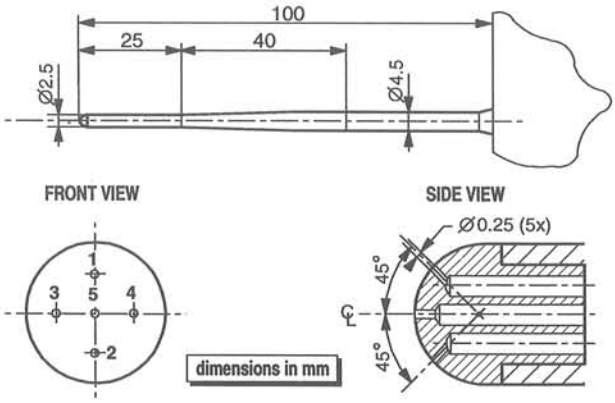

Fig. 4 Five-hole probe geometry

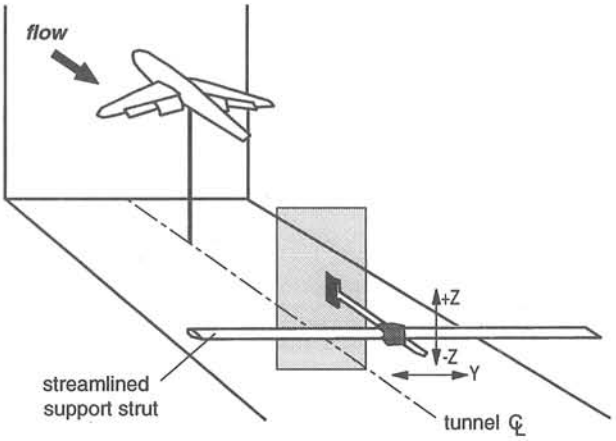

Fig. 5 Model and five hole rake in LST

second. With intermediate traversements at half probe pitch a fine grid (ΔYxΔZ = 5x7.5 mm) is obtained. Dedicated data handling software and interpolation in the calibration data base guarantees a nearly on-line presentation of measured data.

3. DISCUSSION OF RESULTS

3.1 Flow visualisation results

The flow visualisation tests give mainly a qualitative impression of the wake roll-up process up to 5 wing spans downstream of the model. The vortex core trajectories for configurations 2 and 5 are shown in figure 6 and 7, while remaining vortex trajectories in the Yb-Zb cross-plane are shown in figure 8. Concentrated vortices develop from the inboard flap edge, the outboard flap edge and the wing tip. In general the "tip" and "outboard flap" vortex become trapped in a helical motion or even merge at more downstream locations. For high lift (higher angle of attack) the merging process is more rapid than for comparitively low lift cases. However, the vortex from the inboard flap remains well separated from the other two vortices in all cases.

3.2. Flow field measurements

Preliminary (Phase I) flow field measurements confirmed the adequacy of the measurement method. However, the measured cross flow angles (up to 35 deg near vortex cores) were well out of the available calibration range which covered flow angles up to 20 deg. It was therefore decided to recalibrate the rake up to flow angles of 45 deg before the next tunnel entry.

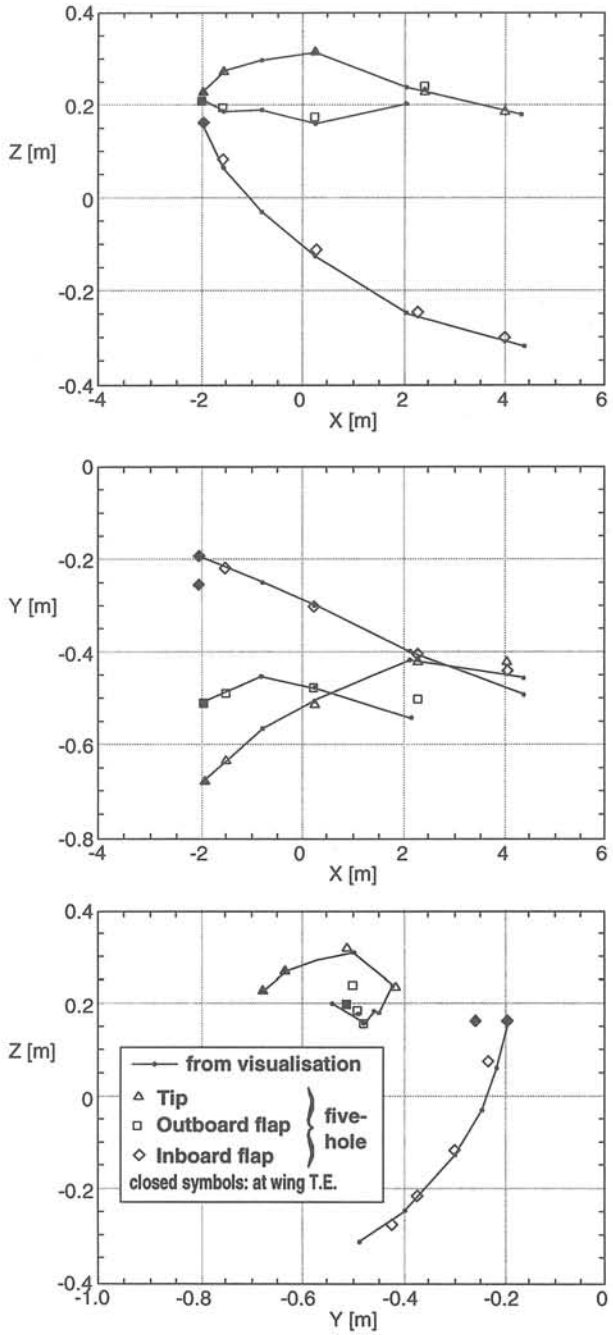

Fig. 6 Location of vortex with respect to test section center for configuration 2, α = 7°

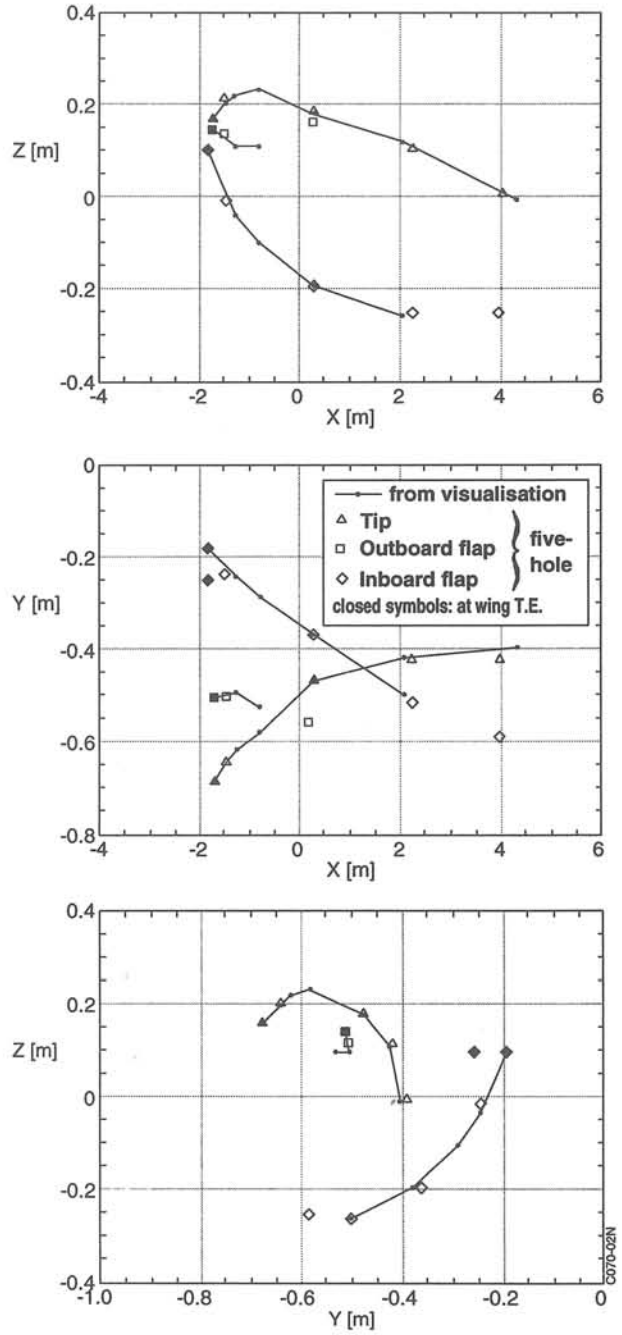

Fig. 7 Location of vortex with respect to test section center for configuration 5, α = 18°

Measurement planes are traversed over two, three or even four rake heights, depending on the vertical extend of the wake region. In total twenty planes were measured, some containing nearly 30000 data points. Though pre-test runs confirmed that the results were not sensitive to traversing direction, all traverses were made starting near Y=-.9 m in the potential flow region outside the wing tip area. Figure 9 shows measured cross flow vectors is a small portion of a measured flow field. It gives a good impression of the observable flow details and the consistency of the measured data. Vortex cores are typically only 20 mm (about 1 % of wing span) in diameter and, despite the small size of the probes, one can not expect very accurate results in the vortex cores.

Prior to further analysis of the measured data, the three components of the non-dimensional velocity vector were linearly re-interpolated in spanwise direction to obtain data on a regular rectangular grid (ΔYxΔZ = 5x7.5 mm). A small spanwise invariant correction on measured velocity components was applied as well (corrections typically 0.5 deg or less). The non-dimensional streamwise vorticity component ω_x (scaling factor U_∞/b):

$$\omega_x = \frac{\partial w}{\partial y} - \frac{\partial v}{\partial z} \qquad (1)$$

was computed with central differencing in velocity components.

Plots 1 and 2 show the downstream development of crossflow velocity and streamwise vorticity fields for configuration 2 (α=7 deg) and configuration 5 (α=18 deg). Note that only a

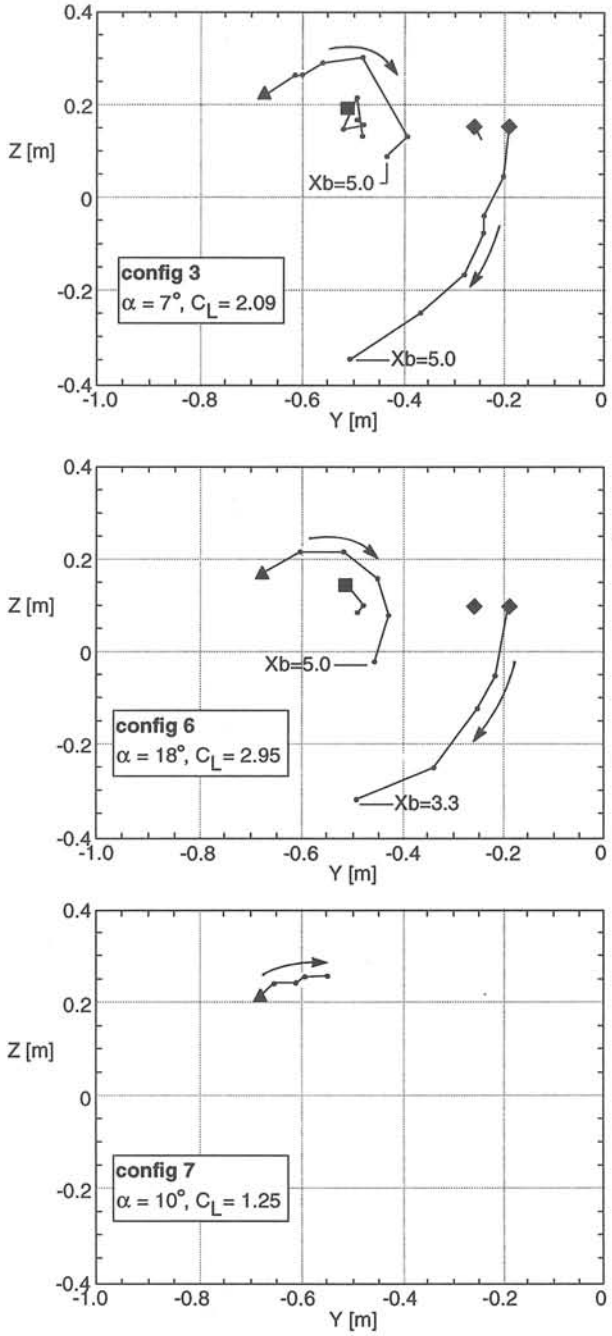

Fig. 8 Vortex core trajectories from flow visualisations

quarter of the available cross-flow vectors is shown for clarity. The position of the vortex cores is in good agreement with the flow visualisation results (see Fig. 6 and 7). Maximum crossflow velocity is seen to grow with model angle of attack (up to 60 % of free-stream velocity for configuration 5, α=18 deg at Xb=.67, see Tab. 3) and decreases in downstream direction. At Xb=.67 the thin vorticity layer emanating from the wing trailing edge and the counter rotating region from the inboard flap edge are clearly visible, while the spanwise position of the individual vortices is still well related to the flap partition geometry of the model. At more downstream stations the vorticity becomes more and more concentrated in individual isolated vortices, though some remnants of the vorticity layer are still seen spiraling around the vortex cores. The weak straight horizontal vorticity layers are clearly unphysical and caused by small probe dependent errors ($\Delta\alpha$ and/or $\Delta\beta$ errors of order one deg, probably due to small oil and/or dust particles occasionally attaching to the probe heads). At more downstream locations the tip and outboard flap vortex tend to merge. The inboard flap vortex and the tip vortex remain however well separated, though for configuration 5, starting from α=12 deg, the distance between these two vortices decreases in downstream direction and with the angle of attack of the model (see Tab. 3).

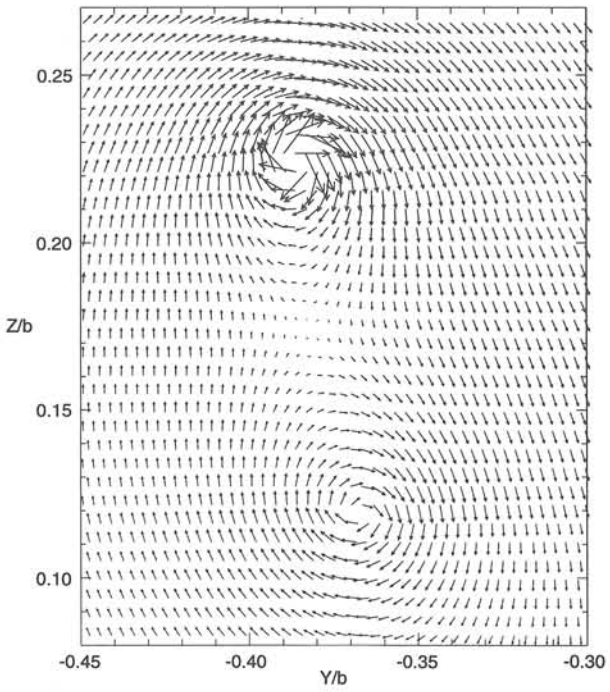

Fig. 9 Measured cross-flow vectors, configuration 2, Xb = 2.0, α= 7°

A good impression of the position of the wake can be obtained by plots of axial velocity. For configuration 5, α=18 deg, results are shown in plot 3. At Xb=0.67 the compartimentation of the flow (high velocities above and low velocities below the wing) is still clearly visible. Just as in Huenecke (Ref. 1) the tip vortex is partly surrounded by a region with comparitively large axial velocity, especially at initial station Xb=0.67 ($u_{max}\approx1.07$). At the Xb=0.67 station the large wake region emanating from the fuselage is clearly visible. At more downstream locations the inboard flap vortex remains embedded in a large region with low speed flow.

3.3. Spanwise wing load and total lift force.

The strength of the trailing vortex system downstream of the configuration is proportional to the wing lift, while its topology will largely depend on the spanwise lift distribution of the wing. According to Maskell (Ref. 2) and Brune (Ref. 3) the total lift and spanwise wing load can be obtained from wake measurements. The contribution of the measured portion of the wake plane to the total lift coefficient becomes (see Fig. 10):

$$C_L = \frac{4b^2}{S}\int_{y_{min}}^{y_{max}}\int_{z_{min}}^{z_{max}}(y\,\omega_x)\,dy\,dz\,,\; y_{max}\le 0 \qquad (2)$$

With Yb in the integrand and no large concentrated vorticity to be expected near the model symmetry plane, Eq. 2 should give a fair approximation of total lift even at Xb=.67 where $y_{max}<0$ due to the presence of the fuselage. Instead of solving Eq. 2 directly, we may also refer to the circulation $\Gamma(y)$ of the bound and trailing vortices. To first order the spanwise wing load is directly related to $\Gamma(y)$:

$$c_l c(y) = 2b\Gamma(y)\,. \qquad (3)$$

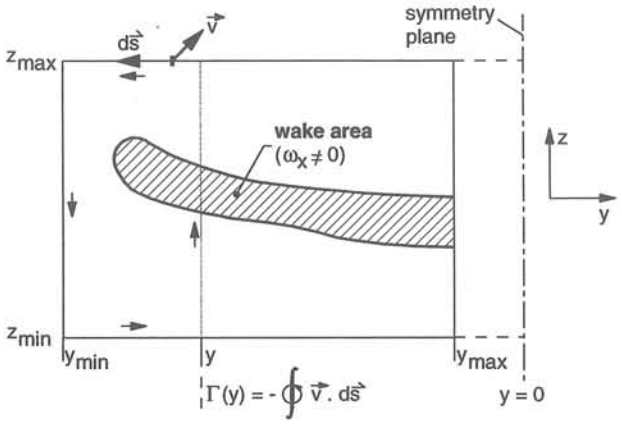

Fig. 10 Domain of integration for model lift

This relation is generally lost at more downstream stations due to the wake roll-up process. Two alternative methods were used to determ Γ(y). In the first method, with $d\Gamma=-\omega_x dydz$, the following expression for dΓ/dy is found:

$$\frac{d\Gamma}{dy} = -\int_{z_{min}}^{z_{max}} \omega_x dz. \qquad (4)$$

Integration in y-direction (taking Γ=0 at $y=y_{min}$) yields Γ(y). In the second method the circulation is determined from a closed contour integration of velocities (see Fig. 10). Eq. 2 can be rewritten to obtain the lift coefficient from a spanwise integration of Γ(y):

$$C_L = -\frac{4b^2}{S}\int_{y_{min}}^{y_{max}}\left(y\frac{d\Gamma}{dy}\right)dy = \frac{4b^2}{S}\left(-y\Gamma\Big|_{y_{min}}^{y_{max}} + \int_{y_{min}}^{y_{max}}\Gamma(y)dy\right), \qquad (5)$$

where $y_{min}\Gamma(y_{min})=0.0$. The total lift was computed with these three alternative methods and differences were less than a few percent, demonstrating the consistency of the present data. Results are compared against direct balance measurements in figure 11. For model configuration 5 the computed lift is largely independent of the measurement plane and the results compare quite well with the direct force measurements. However, less satisfactory results are observed for configuration 2. Spanwise wing load distributions at Xb=.67 are shown in figure 12. The jumps in span-load are an indication for the strength of individual vortices at this position. Note that the spanwise positions of the jumps in circulation do not match with flap partition locations since already some wake roll-up occurred. At low angles of attack the inboard flap vortex is relatively strong, while at high angles of attack the tip vortex gains more importance. Further note that a change of model configuration at α=9 deg (with and without slats extended) hardly affects the wing load distribution.

3.4. Vortex strength

Once the individual vortices are sufficiently separated, an impression of their strength can be obtained by calculating the circulation Γ(r) and the average circulation velocity $V_c(r)=\Gamma(r)/(2\pi r)$ on circular contours around the vortex core (here defined as point with maximum vorticity). For Xb=4.69, the circulation strength variation with angle of attack is shown in figure 13, while V_c is shown in figure 14. Note that lines stop when the circular contour touches the edge of measurement domain. The tip vortex strength continuously increases with angle of attack (partly by the merging proces with the outboard flap vortex), but the strength of the inboard flap vortex remains rather constant up to α=12 degrees and then starts to diminish in strength considerably. At Xb=4.67 the non-

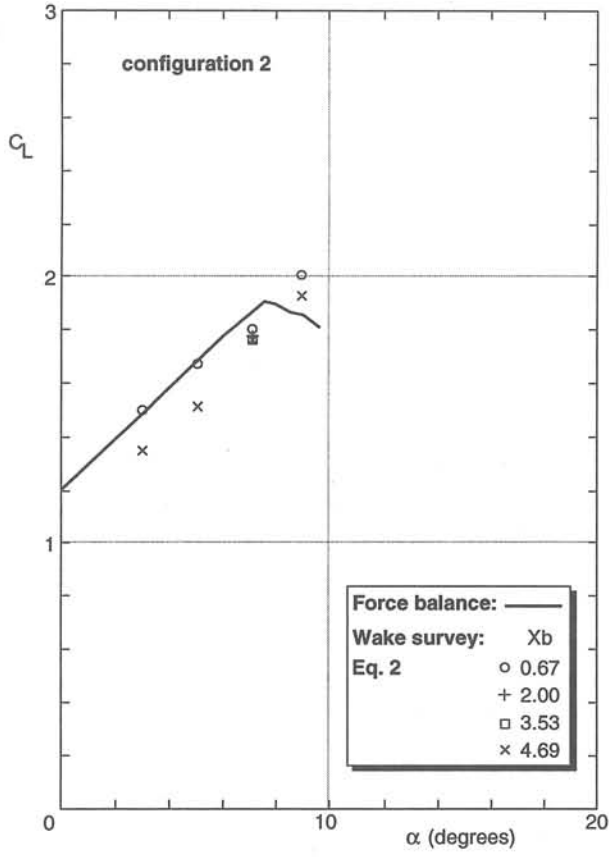

Fig. 11a C_L - α curve, configuration 2

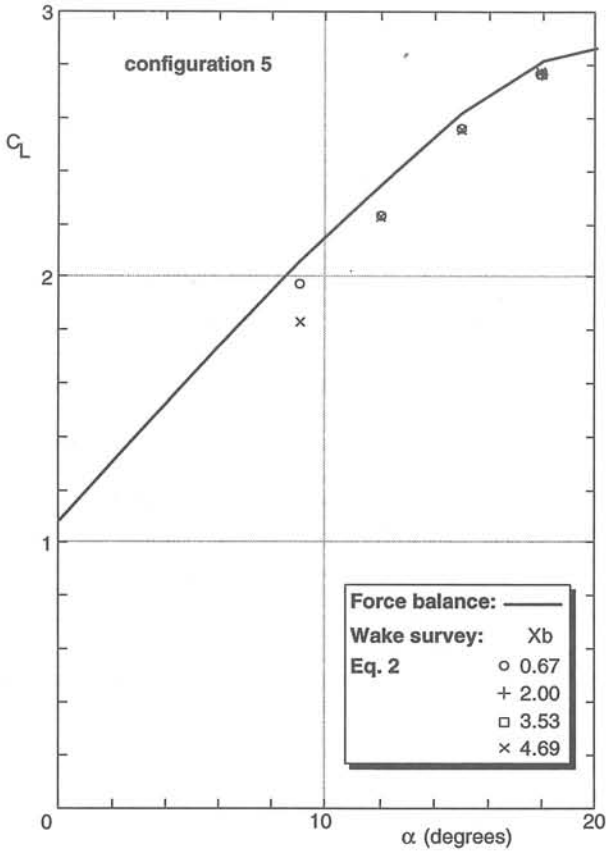

Fig. 11b C_L - α curve, configuration 5

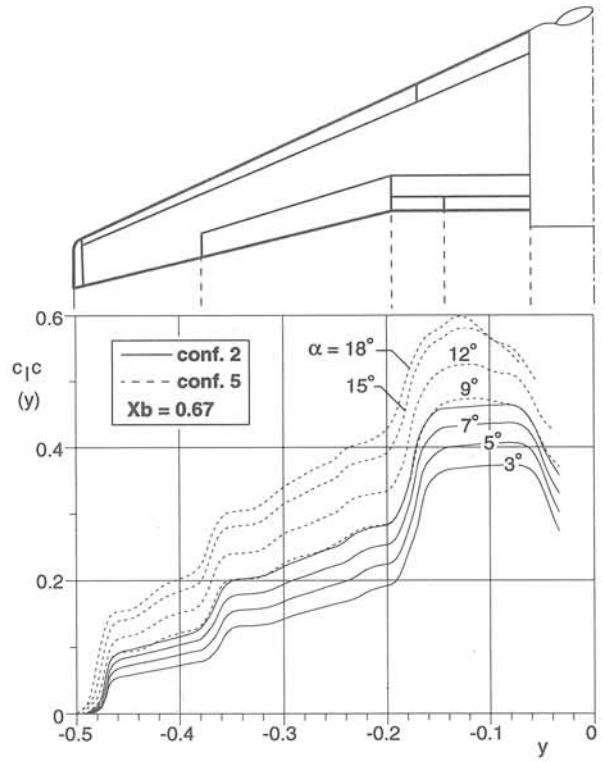

Fig. 12 Spanwise "wing loads" at Xb = 0.67

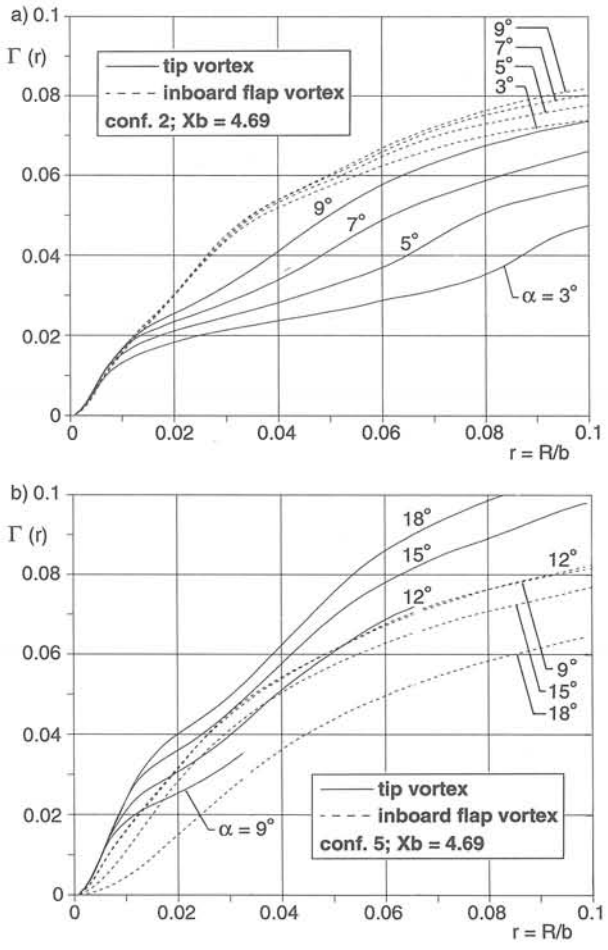

Fig. 13 Vortex strength, variation with α

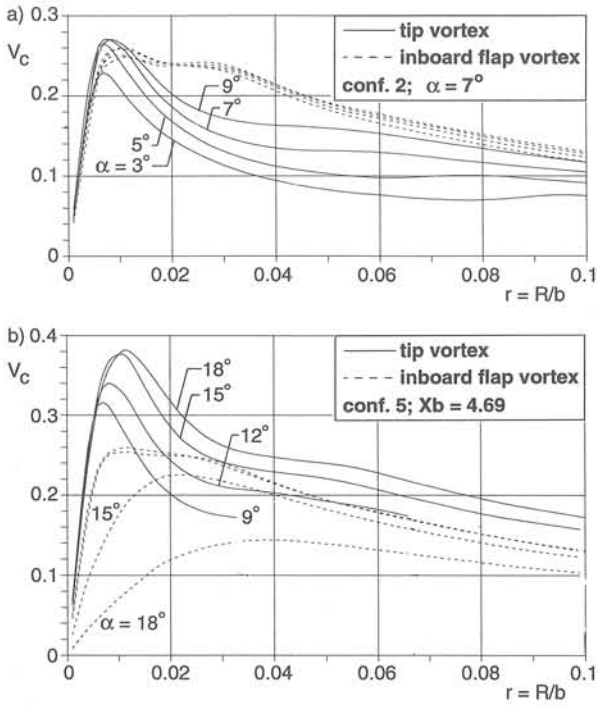

Fig. 14 Mean circulation velocity, variation with α

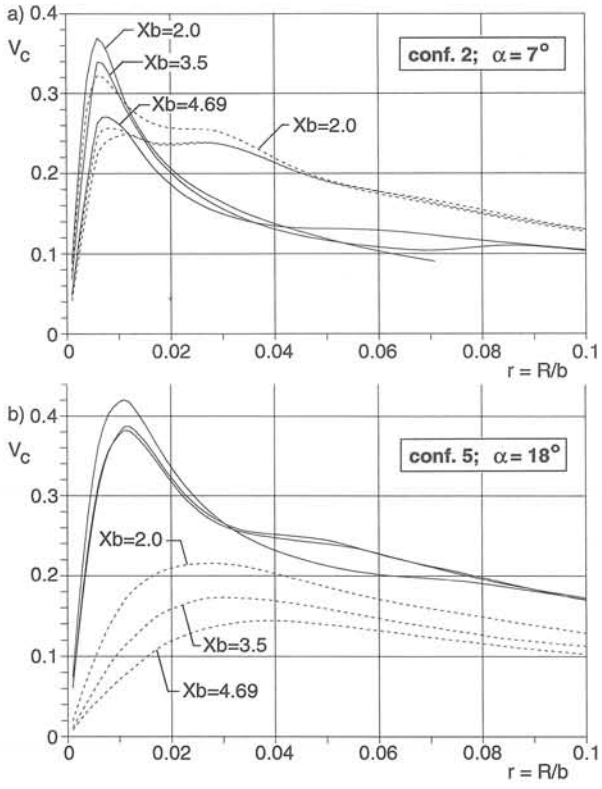

Fig. 15 Mean circulation velocity, variation with Xb

dimensional viscous core diameter of the tipvortex is about 0.015 (20 mm) and largely independent of model angle of attack. On the other hand the viscous core diameter of the inboard flap vortex increases considerably above α=12 deg. The downstream development of V_c, shown in figure 15, reveals a particularly rapid increase of vortex core diameter for the inboard flap vortex (configuration 5, α=18 deg).

4. WAKE ROLL-UP CALCULATIONS

Assuming flow turbulence and vortex stretching effects to be small, the wake roll-up can be described with the two-dimensional vorticity transport equation (Spalart, Ref. 4 and Fell, Ref. 5):

$$\frac{D\omega_x}{Dt} = \frac{\partial\omega_x}{\partial t} + v\frac{\partial\omega_x}{\partial y} + w\frac{\partial\omega_x}{\partial z} = \frac{1}{Re_b}\left(\frac{\partial^2\omega_x}{\partial y^2}+\frac{\partial^2\omega_x}{\partial z^2}\right), \quad (6)$$

with $t \sim x/u_\infty$ and v and w are obtained from a Poisson equation for the stream function Ψ:

$$\frac{\partial^2\Psi}{\partial y^2} + \frac{\partial^2\Psi}{\partial z^2} = -\omega_x, \text{ with:} \quad (7)$$
$$v = \frac{\partial\Psi}{\partial z};\ w = -\frac{\partial\Psi}{\partial y}$$

Tunnel walls can be simulated by using proper inviscid boundary conditions on Eq. 7. Calculations were initiated with the experimentally determined (unsmoothed) vorticity field at Xb=2.0. For configuration 5 calculations proceed up to Xb=4.69 (with and without tunnel walls) and to Xb=17.5 (without tunnel walls), results are shown in plot 4. At Xb=4.69 only a modest effect of the tunnel walls is observed, leading to a small upward shift of the vortex system ($\Delta z \approx 0.065$). The computed vortex locations with tunnel walls are in very good agreement with the measurements. Between Xb=4.69 and Xb=17.5 a continued downward movement of the vortices and a dimishing distance between the two vortices is observed (non-dimensional distance goes from .26 at Xb=4.69 to .18 at Xb=17.5). Calculation results for model configuration 2, α=7 deg., also show a vertical shift ($\Delta z \approx .06$) due to the tunnel wall effect (see plot 5). Again the calculation with tunnel walls shows good overall agreement with experimental results, though there are some differences in the merging of the tip and outbourd flap vortex. It should however be noted that, with these vortices being so close together, the flow becomes particularly sensitive to the initial conditions.

5. CONCLUDING REMARKS

The wake roll-up process behind a high lift configuration of a civil aircraft model with a relatively strong inboard flap was studied up to 5 wing spans behind the model. Mainly model configurations with a powerful 35 deg deflected inboard flap and a mildly 5 deg deflected outboard flap were studied.
With slats extended, a rather large lift coefficient was reached ($C_L \approx 3.0$).

Flow visualisation studies with the laser light sheet method reveal a rapid roll-up of the vorticity layer into individual vortices, emanating from the wing tip, the outboard flap edge and the inboard flap edges. At more downstream locations the wing tip and outboard flap vortices tend to merge, especially for the high lift cases. The wing tip and the inboard flap vortices remain however well separated, though for the higher lift coefficients their mutual distance seems to decrease downstream.

Five hole probes were used to measure the three components of velocity. Twenty planes were measured, each containing 15000 to 30000 individual data points on a fine measurement grid (5x7.5 mm). Crossflow vector plots reveal a complicated structure of the flow field, with small sized vortex cores (typically 20 mm in diameter or even less). Contrary to the tip vortex the inboard flap vortex is imbedded in an area with comparitively low speed flow, especially at higher angles of attack.

Streamwise vorticity was evaluated and Maskell's method was applied to determine the total lift and the spanwise wing load of the model. Results agree reasonably well with force balance measurements. Spanwise lift loadings and detailed analysis of the strength of individual vortices reveal a growing importance of the tip vortex for higher angles of attack. On the other hand the strength of the inboard flap vortex remains fairly constant. However, above α=12 deg the core diameter of the inboard flap vortex rapidly increases downstream.

Measured streamwise vorticities at Xb=2.0 were used as initial data field for wake roll-up calculations with a two-dimensional vorticity transport equation. At Xb=4.69 calculation results with windtunnel walls included are in excellent agreement with experimental vortex locations. Calculations confirm that the disturbing effects due to the tunnel walls are relatively small. For model configuration 5, α=18 deg, calculations were continued up to Xb=17.5 (no tunnel walls). A decrease of distance beween the tip and inboard flap vortices is noted (non-dimensional distance decreases from 0.26 to 0.18 between Xb=4.69 and 17.5), but further analysis is needed whether this is due to a cyclic variation or not.

Additional measurements, up to about Xb=13, are planned in the large low speed windtunnel DNW to increase confidence in the idea that vortices can remain separated up to large distances downstream.

6. REFERENCES

1. K. Huenecke, *"Wake vortex investigations of transport aircraft"*, AIAA-95-1773-CP, 1995.
2. E.C. Maskell, *"Progress towards a method for the measurement of the components of the drag of a wing af finite span"*, RAE Technical Report 72232, 1972.
3. G.W. Brune, *"Quantitative low-speed wake surveys"*, Journal of Aircraft, Vol. 31, No. 2, March-April 1994.
4. Ph. R. Spalart, *"On the motion of aircraft wakes in a stably stratified fluid"*, submitted to JFM.
5. St. Fell and R. Staufenbiel, *"Formation and structure of vortex systems generated by unflapped and flapped wing configurations"*, Z. Flugwiss. Weltraumforsch. 19(1995),

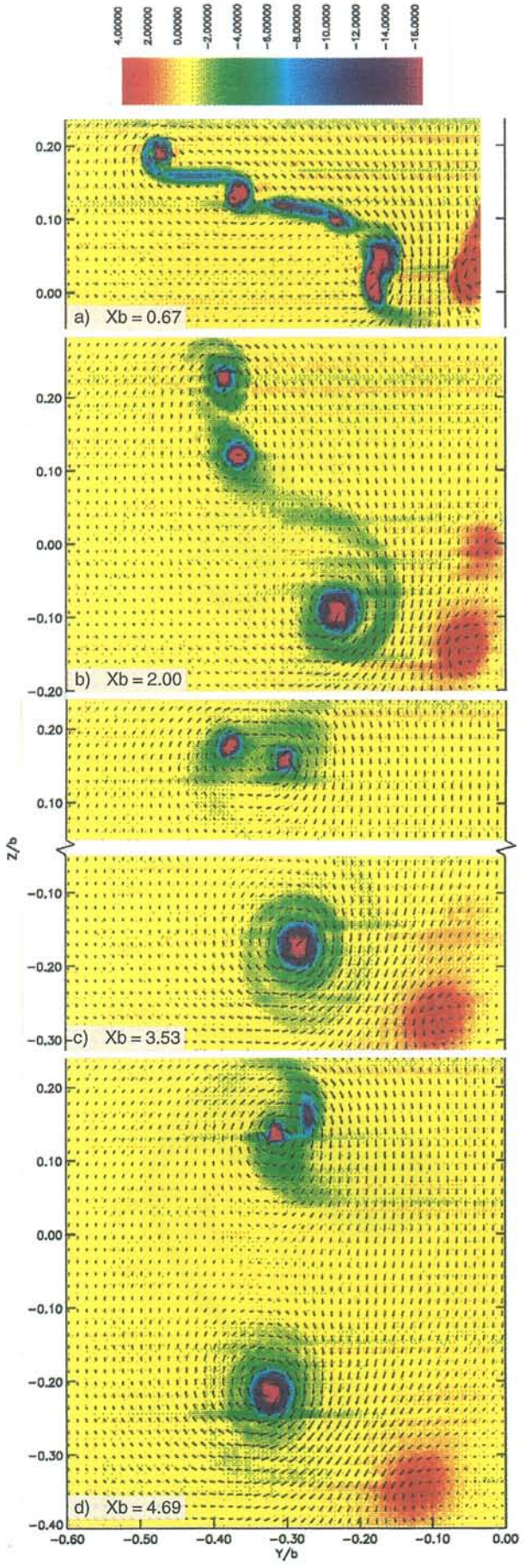

Plot 1 *Downstream development of streamwise vorticity, configuration 2, α = 7°*

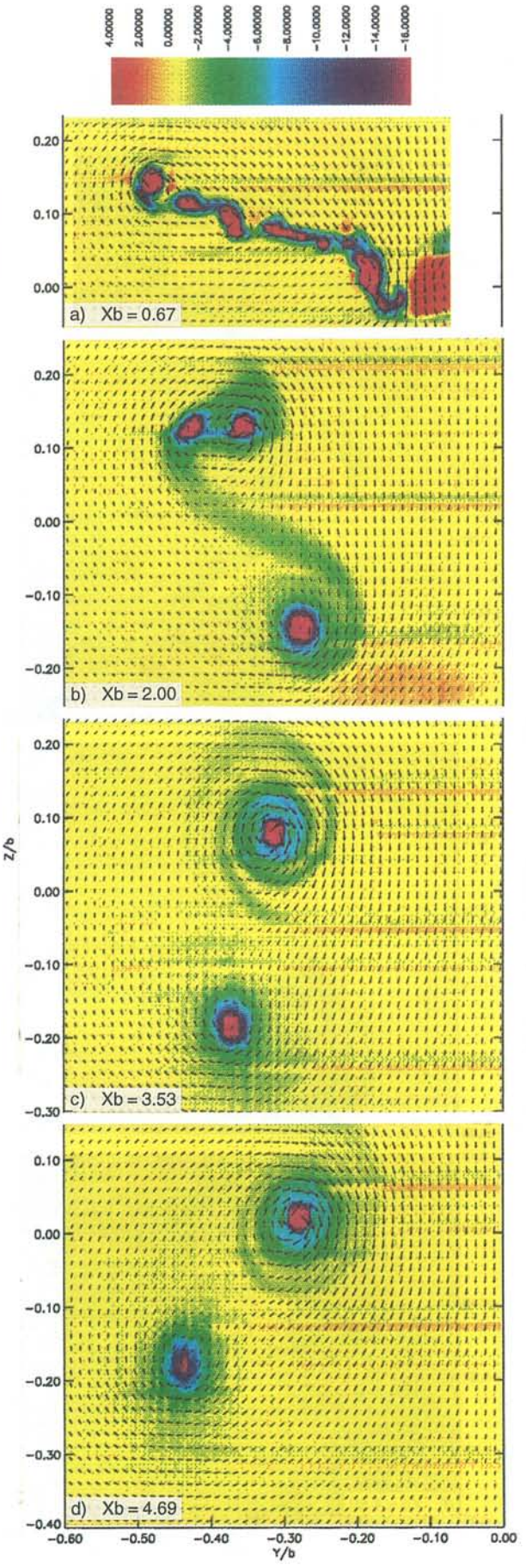

Plot 2 *Downstream development of streamwise vorticity, configuration 5, α = 18°*

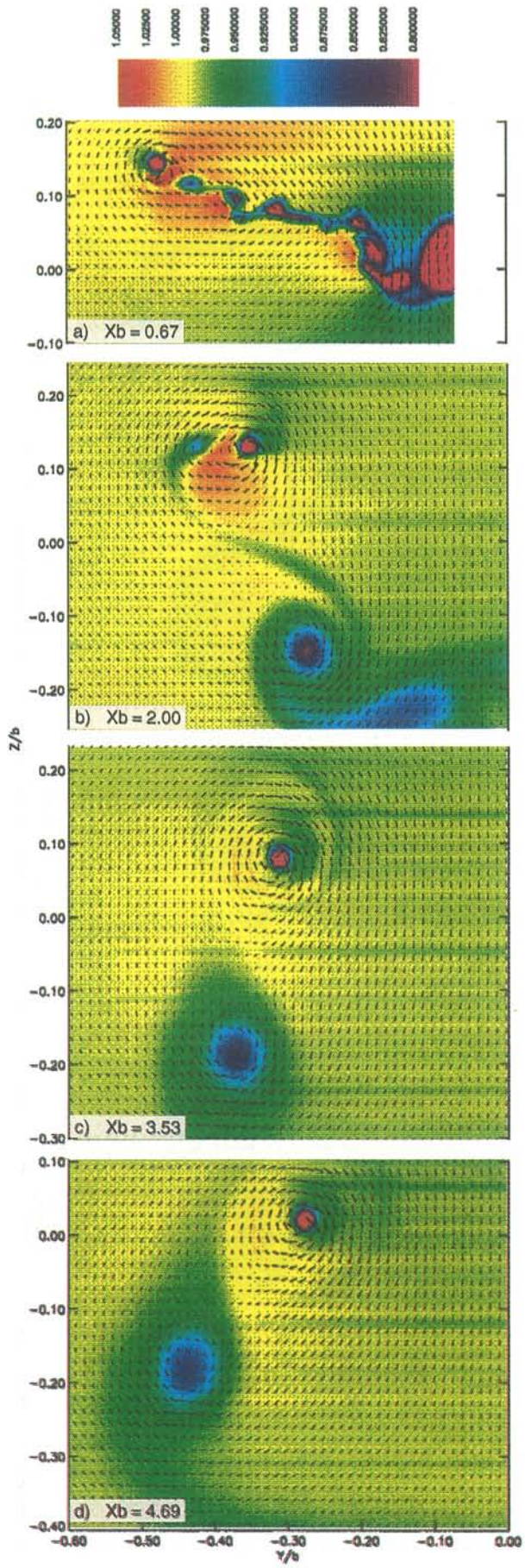

Plot 3 Downstream development of axial velocity, configuration 5, α = 18°

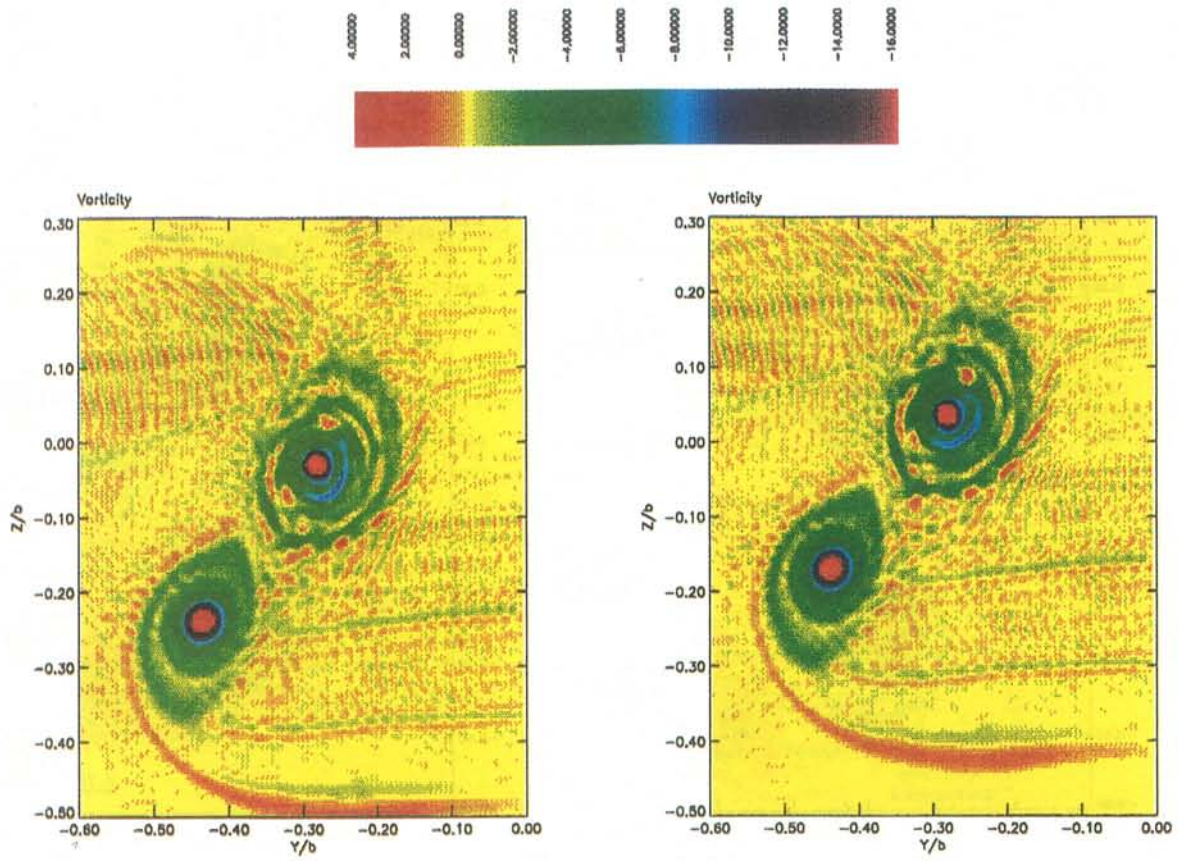

a) Xb = 4.69, no tunnel walls

b) Xb = 4.69, with LST tunnel walls

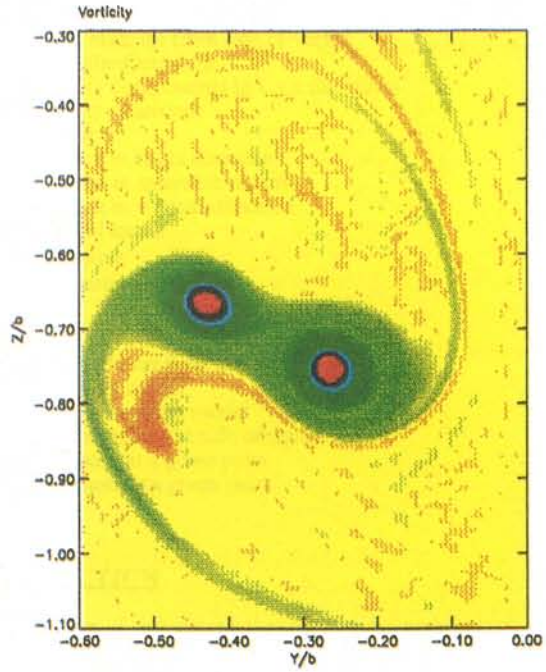

c) Xb = 17.5, no tunnel walls

Plot 4 Computed vorticity fields, configuration 5, α = 18°

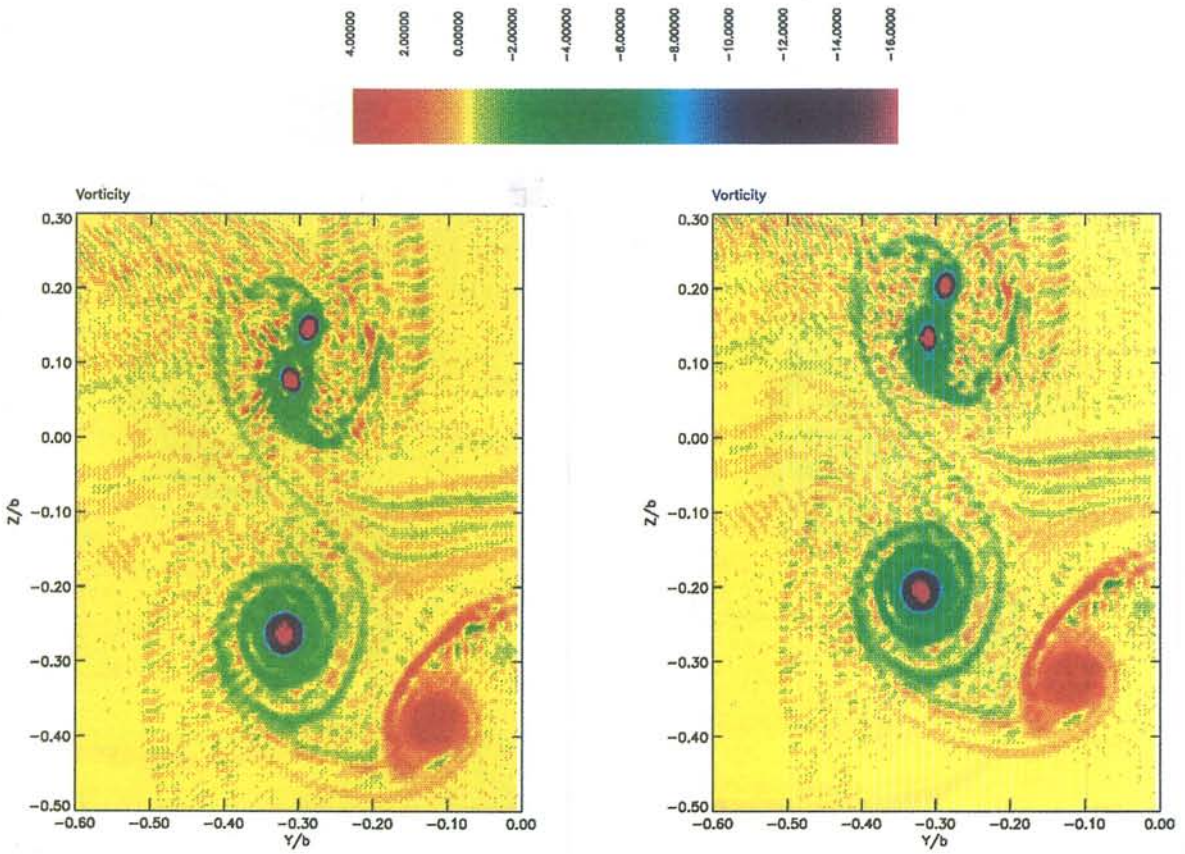

a) Xb = 4.69, no tunnel walls

b) Xb = 4.69, with LST tunnel walls

Plot 5 Computed vorticity fields, configuration 2, $\alpha = 7°$